

Multitip scanning gate microscopy for ballistic transport studies in systems with two-dimensional electron gas

K. Kolasiński,¹ B.Szafran,¹ and B. Hackens²

¹*AGH University of Science and Technology, Faculty of Physics and Applied Computer Science, al. Mickiewicza 30, 30-059 Kraków, Poland*

²*Université Catholique de Louvain (UCL), IMCN/NAPS, 2 Chemin du Cyclotron, 1348 Louvain-la-Neuve, Belgium*

We consider conductance mapping of systems based on the two-dimensional electron gas with scanning gate microscopy using two and more tips of the atomic force microscope. The paper contains results of numerical simulations for a model tip potential with a proposal of a few procedures for extraction and manipulation the ballistic transport properties. In particular, we demonstrate that the multi-tip techniques can be used for readout of the Fermi wavelength, detection of potential defects, filtering specific transverse modes, tuning the system into resonant conditions under which a stable map of a local density of states can be extracted from conductance maps using a third tip.

I. INTRODUCTION

Conductance (G) of open systems with the two-dimensional electron gas (2DEG) in semiconductor heterostructures at low temperatures is determined by scattering of the Fermi level electrons. Using the scanning gate microscopy (SGM) technique¹ one probes the properties of the electron transport in mesoscopic devices by variation of the potential landscape for the Fermi level electrons with the charged tip of the atomic force microscope (AFM) moving above the surface of the sample. The potential of the charge at the tip is screened by the two-dimensional electron gas² which produces a short-range form of the effective tip potential for the Fermi level electrons. The SGM technique was widely used in the studies of the ballistic electron transport, in particular to visualize the electron trajectories as deflected by external magnetic field³, electron branching of the Coulomb flow^{4,5} including an evidence of the quantum Braess paradox⁶, formation of a quantum ring potential with a controlled number of modes in each arm⁷, investigation of electron backscattering with quantum point contacts^{4,5}, formation of Coulomb islands⁸ and mapping the local density of states (LDOS)^{9,10}. Besides the studies of the ballistic flow, the tip potential is also used for the studies of the charge flow in conditions of the Coulomb blockade in quantum dots¹¹. The role of the tip is then to tune the chemical potential of the confined electron system into the transport window defined by the Fermi energies of the source and drain electrodes¹¹.

In this paper we consider possible applications of the SGM technique for the studies of the ballistic

transport using two or more tips instead of a single one. We show that the double tip system can be used to: i) measuring the Fermi wavelength, ii) mapping the potential defects in the channel iii) mode filtering, iv) detection of localized resonances in an experimental implementation of a stabilization method, v) tuning the system to resonant conditions when LDOS can be read-out with a third tip.

Usage of several probes was implemented a few years ago for the scanning tunneling microscopy (STM) studies of the sample surface. A version of the STM technique using several independent tips was used in particular to perform the four point measurements¹² for determination of the surface properties.

II. MODEL

We consider the ballistic transport at the Fermi level electrons in systems based on a two dimensional electron gas (2DEG). We neglect the electron-electron interactions and we use the effective mass Hamiltonian of form

$$\left\{ -\frac{\hbar^2}{2m_{\text{eff}}} \nabla^2 + V_{\text{ext}}(x, y) \right\} \psi(x, y) = E_{\text{F}} \psi(x, y), \quad (1)$$

where $m_{\text{eff}} = 0.067m_0$ is the effective mass of GaAs, E_{F} is the Fermi level energy, and V_{ext} contains all external sources of the electrostatic potential (eg. potential of the tips V_{tip}). We assume that the potential of the tip is given by short-range Lorentzian potential

of amplitude U_{tip} and width w_{tip}

$$V_{\text{tip}}(x, y) = \frac{U_{\text{tip}}}{1 + \left[(x - x_{\text{tip}})^2 + (y - y_{\text{tip}})^2 \right] / w_{\text{tip}}^2}. \quad (2)$$

This form of the potential was evaluated in previous², self-consistent Schrödinger-Poisson calculation. In the following we assume that all the tip potentials have the same width and amplitude and that the distance between them can be changed. The shape of the discussed devices - tailored from the sample containing a two-dimensional electron gas is described by hard-wall boundary conditions.

In order to solve the scattering problem we use a finite difference implementation of the Transparent Boundary Method (TBM)¹³⁻¹⁵. For the boundary conditions in the input lead we use the standard approach with the wave function given by superposition of incoming and outgoing (reflected) transverse modes

$$\psi_{\text{input}}(x, y) = \sum_{k=1}^{M_{\text{input}}} \left\{ a_k e^{ikx} \chi_k^{\text{input}}(y) + r_k e^{-ikx} \chi_{-k}^{\text{input}}(y) \right\}, \quad (3)$$

where M_{input} is the number of current propagating transverse modes χ_k^{input} in the input lead, a_k and r_k are the incoming and reflection amplitudes. For the output lead we assume that the wave function is given by formula

$$\psi_{\text{output}}(x, y) = \sum_{k=1}^{M_{\text{output}}} t_k e^{ikx} \chi_k^{\text{output}}(y), \quad (4)$$

where M_{output} is the number of transverse modes χ_k^{output} in the output lead and t_k is the outgoing amplitude. The transverse modes were calculated with the method presented in Ref.¹⁶. Matching the boundary conditions (3) and (4) with the wave function calculated inside the device one finds the solution for the scattering problem. After solution of the Eq. (1) (for details see¹⁵) for each incoming mode i the conductance of the system is calculated from the transmission probability T_i using the zero-temperature Landauer formalism

$$G = G_0 \sum_{i=1}^{M_{\text{input}}} T_i,$$

with $G_0 = \frac{2e^2}{h}$.

In all the cases considered below we assume that both leads have the same width, thus $M \equiv M_{\text{input}} = M_{\text{output}}$. We choose the discretization grid $\Delta x = \Delta y = 4\text{nm}$. In further discussion we will refer to the local density of states which is defined as the sum of electron densities incoming from the left and right lead².

III. IMPURITIES MAPPING

Let us start our discussion with the device presented in Fig. 1. We consider a long (1000nm) and narrow (80nm) channel. For the Fermi energy $E_F = 2.5\text{meV}$ there is only one current-propagating transverse mode in the channel ($M = 1$). We consider a double tip system assuming that tips move along the x axis. The center of the system of the two tips is denoted by x_{tip} (see Fig. 1). Both tips are separated by a distance of d_{tip} . We assume $U_{\text{tip}} = 5\text{meV}$ and $w_{\text{tip}} = 15\text{nm}$. For a *single* tip with these parameters the conductance of the system is reduced to $G = 0.12G_0$. In Fig. 2(a) we show the result for the conductance G of the system as a function of x_{tip} and the intertip distance d_{tip} for a clean channel. The d_{tip} dependence of conductance reveals a series of resonances separated by distance $\lambda_F/2 \approx 60\text{nm}$, which are related to formation of standing waves between the tips. Thus with the two tips one can probe the Fermi wavelength.

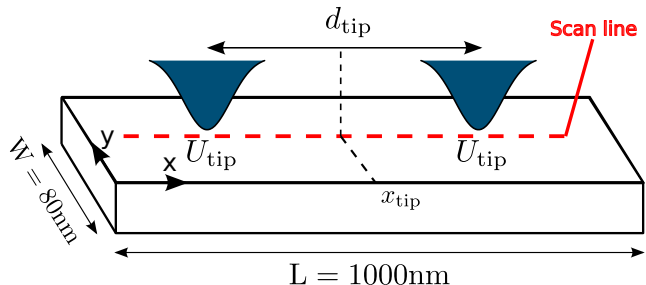


Figure 1: Sketch of the system considered in Sections III and IV. We consider a channel of width $W = 80\text{nm}$ and the system of two tips with the same amplitude $U_{\text{tip}} = 5\text{meV}$ and width $w_{\text{tip}} = 15\text{nm}$. The length of the computational channel is $L = 1000\text{nm}$. The tips are above the axis of the channel (red dashed line) and are separated by a distance d_{tip} . The center of the system of two tips is located at position x_{tip} .

Let us now consider the system with a single potential defect present in the middle of channel. The defect is modeled with Eq. (2) with $U_{\text{imp}} = 2\text{meV}$

and $w_{\text{imp}} = 10\text{nm}$ (see the potential profile below the Fig. 2(b)). Now the SGM image reveals new features - the resonance lines bend and oscillate in the vicinity of the impurity. Far from the impurity the resonance lines return to the same position as in Fig. 2(a). Note that the first resonance line (around the $d_{\text{tip}} \approx 90\text{nm}$) resemble the potential profile inside the channel. In Fig. 2(c,d) we show that the first resonance line follows the potential profile of the defect. This effect can be explained in terms of the semi-classical WKB approximation. For slowly varying potential $U(x)$ and $E_F > U(x)$ the wave vector of propagating wave function $e^{\pm ik_F x}$ is given by $k_F = \sqrt{2m_{\text{eff}}(E_F - U(x))/\hbar}$. Now if $U(x) > 0$ the phase of the wave propagating through the potential hill will be delayed by some value $\Delta\psi$ in comparison to the phase of the unperturbed system. Thus in order to restore the resonance for standing wave one must increase the distance between the tips, by the value which compensates for the delayed $\Delta\psi$ phase. For $U(x) < 0$ the distance between the DT has to be decreased (see Fig. 2(d)).

The system of a single tip and a repulsive defect is equivalent to the double-tip system, hence the position of the defect can be resolved by a scan of a single-tip by a shift of the energy lines. Nevertheless, in order to extract the profile of the potential of a defect one needs two tips and not a single one.

In Fig. 3 we show the results for the channel with two impurities (same as in Fig. 2(c)) but for higher energies E_F . At higher energies [Fig. 3(a)] the resolution of the images is reduced with the resonance lines getting closer and wider, but the image still allows one to map the defect potential distribution along the channel. Note that in Fig. 3(a) we notice the resonances of Fig. 2(c) for both the lowest subband (resonance sequence starting near $d_{\text{tip}} \simeq 30\text{ nm}$) and the second transverse mode (the sequence starts for $d_{\text{tip}} \simeq 100\text{ nm}$). For $E_F = 7.5\text{meV}$ (see Fig. 3(b)) the image loses the features visible in Figs. 2, but the W shaped line clearly indicates the position of the defects.

For completeness we considered a clean channel with the width of the tip potential increased to $w_{\text{tip}} = 50\text{nm}$. In Fig. 4 we plotted the conductance as a function of the intertip distance d_{tip} and the height of the tip potential. For $U_{\text{tip}} = 2\text{ meV}$ the system is transparent for the electron flow, formation of the resonances as discussed above for $w_{\text{tip}} = 15\text{ nm}$ appear higher in the energy and for $U_{\text{tip}} > 3.5\text{ meV}$ the ballistic electron flow is blocked. For larger values of U_{tip} formation of a quantum dot supported by the tips

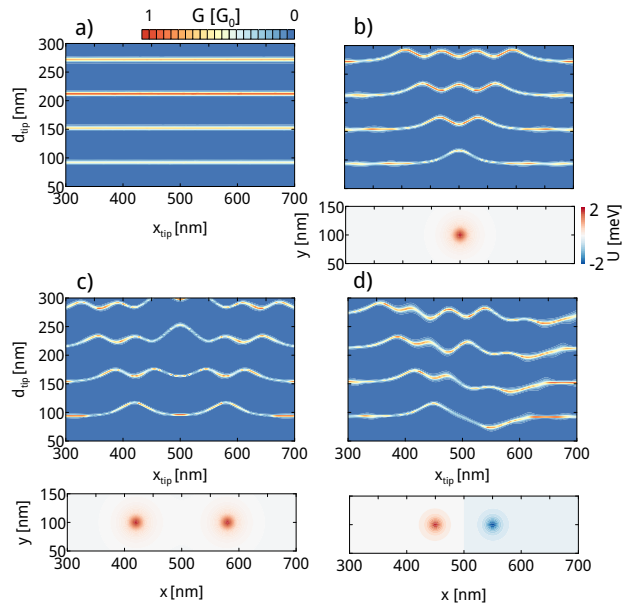


Figure 2: Results for $E_F = 2.5\text{meV}$ (one band transport) a) The DT scan obtained for a clean channel. b) Added impurity in the middle of channel with amplitude $U_{\text{imp}} = 2\text{meV}$ and of width $w_{\text{imp}} = 10\text{nm}$ modeled with Eq. (2). c) the same but for two impurities separated by distance 160nm and d) obtained for two impurities of different sign $\pm 2\text{meV}$ separated by distance 100nm . Plots below show the potential profile in the channel for each case (b-d).

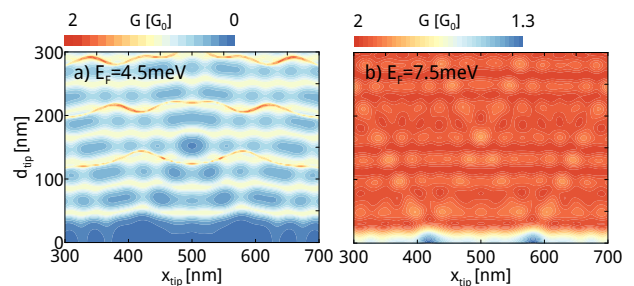


Figure 3: The same as in Fig. 2(c) but for higher Fermi energies. a) Results for $E_F = 4.5\text{meV}$ (two band transport) and b) $E_F = 7.5\text{meV}$.

should be expected with the transport dominated by the Coulomb blockade, which is however, outside the scope of the present work. The best resolution of the scan as a function of d_{tip} is obtained just below the cutoff of the ballistic transport.

To conclude this Section, we find that double tip

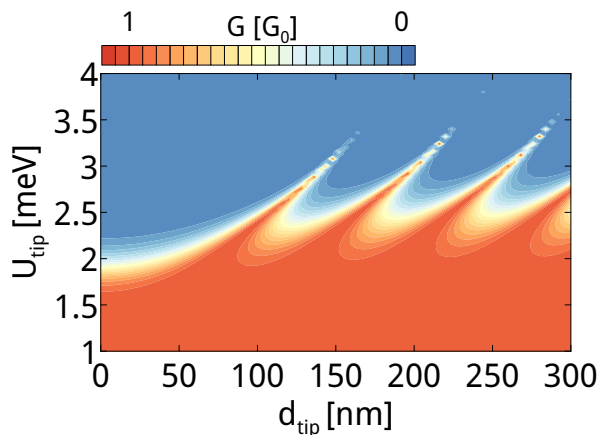


Figure 4: Conductance of the system as a function of the tip amplitude U_{tip} and distance d_{tip} between the tips obtained for $E_F = 2.5\text{meV}$ and width of the tip potential $w_{\text{tip}} = 50\text{nm}$.

system can be used to read out the Fermi wavelength and the potential profile along the channel.

IV. TRANSVERSE MODE FILTER

In Fig. 3(a) we observed the resonances of the first and second subband (the red lines near $d_{\text{tip}} = 100, 200$ and 300 nm). These resonances occur separately or in overlap with the lines of the lowest resonance depending on the values of d_{tip} and x_{tip} . Thus choosing a proper value of d_{tip} and x_{tip} one can make a device which will filter out specific modes. For the proof of principle, we will restrict our consideration to the first and second mode. The resonance lines are plotted in Fig. 5(a) as functions of the distance between the tips and the Fermi energy for the clean channel (as in Fig. 1) but with the width increased to $W = 100\text{nm}$. At low Fermi energies only the first transverse mode is present in the conductance, and the double tip stops the transport unless the Fermi energy coincides with the resonances localized between the tips. For higher values of E_F the resonance lines of the second mode appear and at lines in the (d_{tip}, E_F) plane which intersects with the first mode lines. The images (b-f) in Fig. 5 show the electron density for work points marked by arrows in Fig. 5(a). We can see that for a given energy E_F one may filter out a specific transverse mode, by changing the d_{tip} distance.

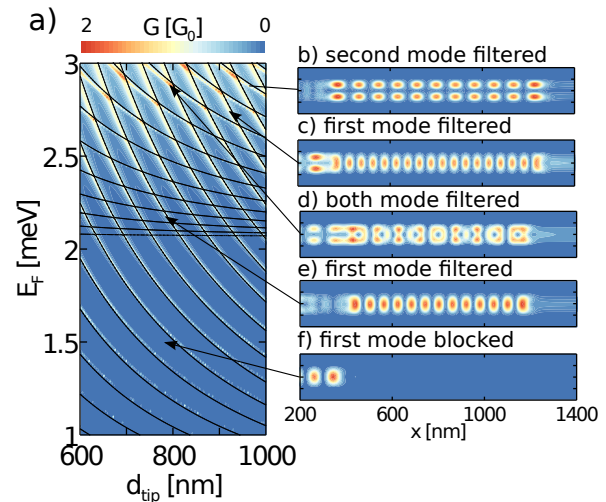


Figure 5: a) The conductance G of the long channel of width $W = 100\text{nm}$ as a function of d_{tip} and E_F . Dashed lines deposited to the (a) shows the energy spectrum a two-dimensional quantum well of length $d_{\text{tip}} - 2w_{\text{tip}}$. The shift by $2w_{\text{tip}}$ accounts for the finite size of the tip potential. (b-f) Electron density $|\psi|^2$ obtained for values of (d_{tip}, E_F) pointed by arrows.

In Fig. 5(a) we plotted the energy spectrum of an infinite quantum well of width 100 nm and length $d_{\text{tip}} - 2w_{\text{tip}}$. The conductance resonances follow exactly the energy spectrum for a infinite quantum well.

V. DETECTION OF LOCALIZED RESONANCES

Let us now consider the system depicted in Fig. 6 with a channel of width 100nm connected to the quantum cavity of length 500nm and width W . In order to get the best resolved images we set the $E_F = 2\text{meV}$ (single subband transport within the channel). In Fig. 7(a) we show the conductance of the system as a function of the d_{tip} and width W of the cavity. We kept the center of the double tip fixed in the middle of the resonant cavity. For small values of W around 100nm the resonance lines are very similar to those of Fig. 5(a). For a changed width of the cavity the cavity-localized energy levels vary as $\propto W^{-2}$. Thus changing the width W we should expect behavior of the resonance lines similar to the ones of Fig. 5(a). Large values of W lead to a complex behavior of the

resonance lines but with well distinguishable patterns of X-shaped lines which appear with a period of λ_F along d_{tip} axis.

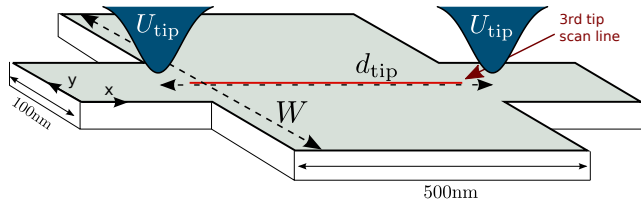


Figure 6: Sketch of the second system considered in this paper. Long channel of width 100nm is coupled to the resonant cavity of variable width W and length 500nm. The same as before we have two tips in the system one in the left lead and second in the right lead. Both tips have the same parameters of $U_{\text{tip}} = 5\text{meV}$ and $w_{\text{tip}} = 15\text{nm}$ and are separated by distance d_{tip} . Red line corresponds to the third tip scan discussed in the last paragraph.

In Fig. 7(b) we show the conductance of the system without the tips. The conductance contains a series of sharp resonances of a Fano type corresponding to quasi-bound states localized within the cavity. Most of the resonances visible in Fig. 7(b) are also present in Fig. 7(a) as nearly horizontal lines – independent of the distance between the tips – which suggests that they correspond to the quasi-localized states of the cavity. The nearly horizontal lines are very thin indicating a long lifetime of the resonances. The lines with a steeper dependence on d_{tip} in Fig. 7(a) correspond to resonances supported by the tips. The lines are wide - indicating a stronger coupling to the channel. A study probing the conductance as a function of the distance between the tips would be an experimental implementation of the stabilization methods¹⁷ for detection of localized resonances.

The zoom of region of the Fig. 7 marked by the black rectangle is depicted in Fig. 8(a). In this picture we can distinguish three types of resonance lines: a) vertical – almost independent of the width W of the cavity, b) resonances which vary with W and c) well visible horizontal resonances – independent of the distance between DT which correspond to the quasi localized state in the cavity. We found in general that the difference between the two first types of resonances come from the symmetry of the resonant scattering densities. The scattering densities for lines of type a) and b) are symmetric with respect to the center of the cavity in the x direction. The resonances that are independent of W have a nodal surface at the symmetry axis, while the other have a maximum on the

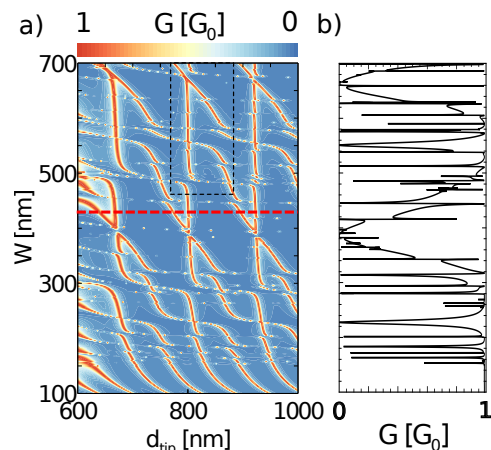


Figure 7: a) The conductance of the system depicted in Fig. 6 as a function of d_{tip} and cavity width W . Dashed rectangle corresponds to the zoomed area shown in Fig. 8(a). Red line corresponds to scan with third tip discussed in the next paragraph. (b) Conductance of the system presented in Fig. 6 as a function of W but without DT.

symmetry line. The former are strongly localized in the center of cavity (see Figs. 8(b-e)) and the latter form resonances which are delocalized over the entire cavity (see Figs. 8(f-g,i)). The delocalized resonances react stronger to the value of W in Fig. 7(a). Fig. 8(h) shows a resonance of a third type - of the energy that is weakly dependent of d_{tip} – which corresponds to the resonances supported by the cavity itself.

In experiments variation of the geometry of the cavity can be accomplished by tuning an electrostatic confinement in the y direction due to external gating. Since the electrostatic confinement potential is usually parabolic at its origin we replaced the hard wall confinement by

$$U_{\text{parabolic}} = \frac{1}{2}\omega'^2 y^2 = \frac{1}{2}(3\text{meV} - \omega)^2 y^2. \quad (5)$$

With this potential the effective width of the cavity is controlled by the harmonic oscillator energy. The parametrization was chosen in order to get better comparison with Fig. 7. The value $\omega = 3\text{meV} \Rightarrow \omega' = 0\text{meV}$ corresponds to a small value of W in Fig. 6 and channel-like behavior of conductance. Value $\omega = 0\text{meV} \Rightarrow \omega' = 3\text{meV}$ corresponds to the large values of W . Comparing the images Fig. 7 and Fig. 9 we can see that both share the same features: a) X-shaped resonance lines are present, b) some resonances depend weakly on W as a function of the cavity width

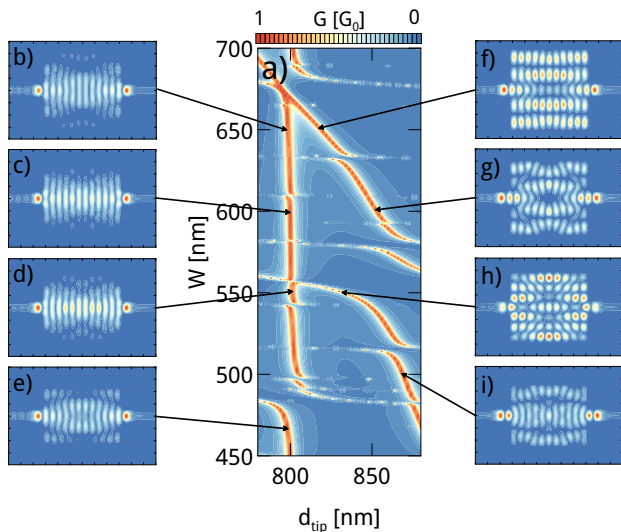


Figure 8: (a) Zoom of figure 7(a) marked by the dashed rectangle. (b-i) Probability density for the electron incoming from the left for d_{tip} and W pointed by the arrows. (b-e) Antisymmetric resonances (f-i) symmetric resonances.

(antisymmetric ones) and some vary with d_{tip} (symmetric states), c) horizontal resonance lines are also present. Note that in this case we do not find the vertical resonances in the conductance image. This is because the variation of ω changes the potential profile in whole cavity and not only the width of the cavity (as it was in the previous example).

Concluding this Section, we found that using double tip system with the cavity of variable width one may tune the system to the specific resonance i) symmetric or antisymmetric resonances supported between the tips ii) or resonances quasi-localized within the cavity (horizontal lines in Figs. 7 and 9).

VI. MAPPING THE LOCAL DENSITY AT FERMI LEVEL

Let us now discuss the possibility of mapping the LDOS inside the device presented in Fig. 6. In the two-dimensional systems the conductance maps can be correlated to the local density of states for weak tip perturbation when the electron scattering wave functions incoming from the left and right leads are the same up to a constant phase. The latter case can be supported¹⁸ by the perturbation theory^{19,20} for which

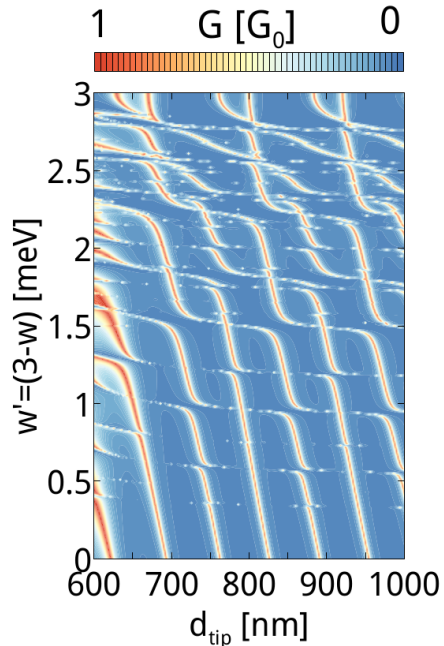


Figure 9: The conductance of the system depicted in Fig. 6 as a function of d_{tip} and angular frequency ω of the oscillator. The parametrization $\omega' = 3\text{meV} - \omega$ is applied in order to keep the same interpretation of y axis (width of the cavity) as in Fig. 7(a).

the first-order correction to the conductance is simply proportional to the LDOS. The scattering densities for the electron incoming from the left lead plotted in Fig. 8(b-i) are highly symmetric since they correspond to the resonances induced by the double tip system in a symmetric cavity. Thus for inverted current direction the scattering density inside the cavity stays the same and this should lead good correlation between LDOS and corresponding G map. In general we find^{2,18} that the correlation LDOS- G is well resolved near the Fano resonances.

In the following calculation we assume that the distance between the two tips placed within the channel is set to a resonance, and the third tip scans the surface of the cavity for detection of the resonant LDOS. The assumed third tip parameters are $U_{\text{tip}} = 1\text{meV}$ and $w_{\text{tip}} = 10\text{nm}$. We need a pronounced variation of G as a function of the tip position and the adopted height of the tip potential is quite large as compared to the Fermi energy kept at 2 meV.

In Fig. 10(a) we show the conductance of the sys-

tem depicted of Fig. 6 as a function of distance between the two tips inside the channels d_{tip} (see Fig. 7) and position of the third tip x_{tip} along the red line in Fig. 6. We observe a number of resonances for a sequence of the tip positions. The resonances appear in pairs, which have LDOS with a minimum or a maximum at the symmetry axis of the device [Fig. 10(c)] with either a maximum or a zero of LDOS at the symmetry axis $x_{tip} = 800$ nm. The d_{tip} distance which corresponds to resonances can be deduced from the conductance dependence of the cavity – double tip system (without the third tip) which is plotted in Fig. 10(d). In Fig. 10(b) we present the deviation ΔG from the conductance G' of the system without the third tip. Note that ΔG changes sign in the vicinity of the resonance induced by double tip (see the blue curve in Fig. 10(d)), which will lead to a negative correlation of between the LDOS and G map¹⁸. In order to compare the conductance obtained from scan with third tip $G_{scan} \equiv G(x_{tip}, d_{tip})$ with the LDOS on that line $L_{scan} = \text{LDOS}(x_{tip}, d_{tip})$ (for given value of d_{tip}) we calculate the Pearson correlation $r \equiv r(d_{tip})$

$$r = \frac{\int (G_{scan} - \langle G_{scan} \rangle)(L_{scan} - \langle L_{scan} \rangle) dx_{tip}}{\Delta_L \sigma(G_{scan}) \sigma(L_{scan})}, \quad (6)$$

where $\langle a \rangle = \frac{1}{\Delta_L} \int a(x_{tip}) dx_{tip}$ is the average value of a , $\sigma^2(a) = \frac{1}{\Delta_L} \int (a(x_{tip}) - \langle a \rangle)^2 dx_{tip}$ is standard deviation of a and $\Delta_L = 800$ nm is the length of the scan along red line in Fig. 6. Before the calculation of r both functions G_{scan} and L_{scan} were normalized to range from 0 to 1. The absolute value of the correlation r is plotted in Fig. 10(d). Note that r increases to about 0.9 near the induced resonances which means that obtained G map well resolve the LDOS inside the cavity. The dips in $r(d_{tip})$ dependence result from the fact that the correlation coefficient changes sign at the resonances¹⁸. In Fig. 11 we present the SGM images and corresponding LDOS for points A, B and C of Fig. 10(d). Summarizing, the usage of multiple tips allows for 1) tuning the system to a resonance and then 2) an accurate read-out of the local density of states.

For evaluation of the LDOS we normalized the scattering densities to the unity within the computational box. For off-resonant conditions, where the scattering density is large only inside the input and output channels, we thus obtain a strong reduction of LDOS within the cavity. This normalization approach gives a close correspondence of LDOS with SGM maps for varied d_{tip} and x_{tip} [cf. Fig. 10]. For fixed values of these parameters, the Pearson correlation coefficients

between the maps is not affected by the LDOS normalization.

VII. TIP AS A PART OF THE SCATTERING SYSTEM

The scanning gate microscope tip can be used as a part of the scattering system, with the other tip gathering the conductance maps. In particular, the tip potential placed near the exit of the quantum point contact has been used to form a quantum Hall interferometer²¹. A similar quantum Hall system including a potential defect spontaneously formed at the exit from the QPC constriction was studied with the scanning gate microscopy in Ref.²²

The SGM with a double tip system can be used for observation of the Young interference²³ for a set-up depicted in Fig. 12. The SGM signal was predicted²³ to contain signatures of the double-slit interference for low-energy transport. The proposed²³ set-up requires a beam splitter – a central obstacle for the electron flow, which may be difficult to introduce in form of a fixed gate. A floating one – introduced by the tip – is a possible option. In Fig. 12 we plotted a system with the QPC slit entering a small open cavity. The potential of the tip (schematically shown with the gray circle) was introduced near the exit of the cavity to an unconfined half-plane. The scattering density current $|j(x, y)|$ plot in Fig. 12 shows formation of the interference pattern characteristic for the Young interference²³. The other tip used as an electron flow detector could then be used for readout of the double-slit interference in the SGM conductance images.

VIII. CONCLUSIONS

We have studied numerically the possible applications of the multitip scanning gate microscopy on the systems with 2DEG. We found that the measurements using a pair of tips allows for 1) readout of the Fermi wavelength 2) detection of the potential defects with indication of their position and profile, 3) filtering of specific transverse modes 4) tuning the system into a resonance that allows for a reliable detection of the local density of states with a third tip.

Acknowledgments This work was supported by National Science Centre according to decision DEC-2012/05/B/ST3/03290, and by PL-Grid Infrastructure. The first author is supported by the scholarship

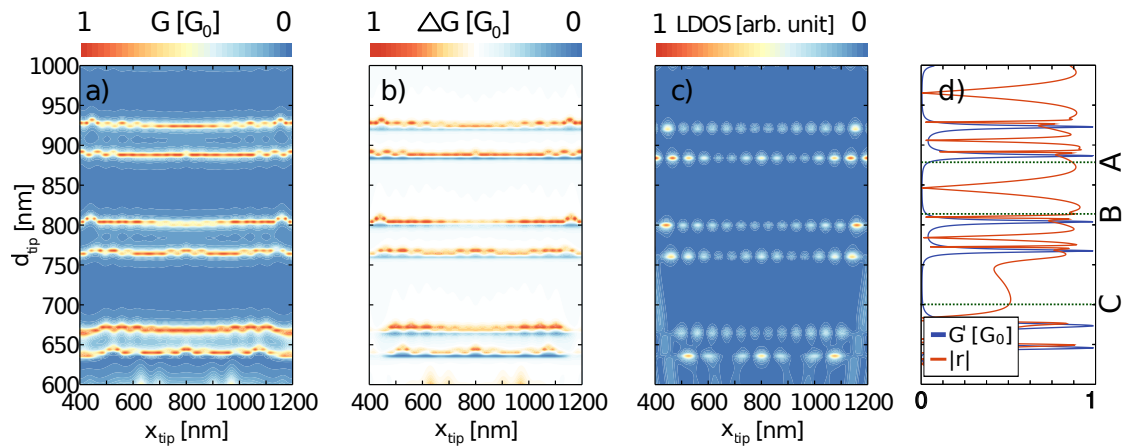


Figure 10: a) Conductance G of the system as a function of third tip position x_{tip} (moved along the red line in Fig. 6) and distance between the two tips (red line in Fig. 7(a)) b) The same but $\Delta G = G - G'$ is plotted, where G' is the conductance of the system without the third tip c) is the LDOS. d) (blue line) Conductance G' of system as a function of d_{tip} without third tip. (red line) Absolute value of Pearson correlation r between (a) and (c) images calculated from Eq. 6.

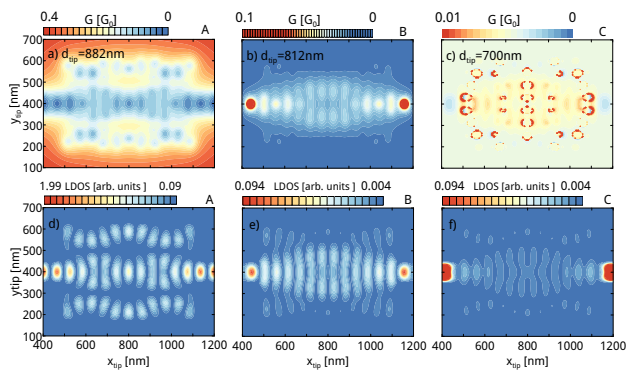


Figure 11: a-c) The SGM image d-f) and LDOS obtained for point **A**, **B** and **C** in Fig. 10(d). Point **A** corresponds to the symmetric resonance induced by the double tip system in work point where the correlation r is negative. Point **B** corresponds to the antisymmetric resonance with positive correlation r . Point **c** corresponds to a zero of T in the absence of the tip.

of Krakow Smoluchowski Scientific Consortium from the funding for National Leading Research Centre by Ministry of Science and Higher Education (Poland).

¹ H. Sellier, B. Hackens, M.G. Pala, F. Martins, S. Baltazar, X. Wallart, L. Desplanque, V. Bayot, and S. Huant, Sem. Sci. Tech. **26**, 064008 (2011); D.K. Ferry, A.M. Burke, R. Akis, R. Brunner, T.E. Day, R. Meisels, F. Kuchar, J.P. Bird, and B.R. Bennett, Sem. Sci. Tech. **26**, 043001 (2011).

² K. Kolasiński, B. Szafran Phys. Rev. B **88**, 165306 (2013)

³ Aidala, Katherine E.; Parrott, Robert E.; Kramer, Tobias; et al., Nature **3**, 7 (2007)

⁴ M. A. Topinka, B. J. LeRoy, S. E. J. Shaw, E. J. Heller, R. M. Westervelt, K. D. Maranowski, and A. C. Gos-

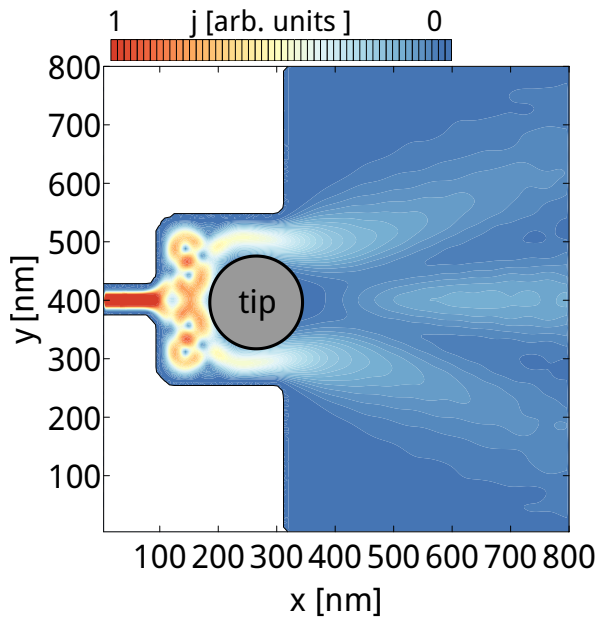


Figure 12: Schematics of system with a quantum point contact and the tip potential for observation of the Young interference and the calculated scattering density current $|j(x, y)|$ including the double-slit interference pattern. The applied tip potential parameters: $w_{\text{tip}} = 50\text{nm}$ and $U_{\text{tip}} = 10\text{meV}$

- sard, *Science* **289**, 2323 (2000).
- ⁵ M. A. Topinka, B. J. LeRoy, R. M. Westervelt, S. E. J. Shaw, R. Fleischmann, E. J. Heller, K. D. Maranowski, and A. C. Gossard, *Nature* **410**, 183 (2001).
- ⁶ Pala, M. G.; Baltazar, S.; Liu, P.; et al., *Phys. Rev. Letters* **108**, 6 (2012); A. A. Sousa, Andrey Chaves, G. A. Farias, and F. M. Peeters; *Phys. Rev. B* **88**, 245417 (2013)
- ⁷ Kozikov, A. A.; Steinacher, R.; Roessler, C.; et al., *New J. Phys.* **16**, 053031 (2014)
- ⁸ Hackens, B.; Martins, F.; Faniel, S.; et al., *Nature Communications* **1**, 39 (2010)
- ⁹ Sellier, H.; Hackens, B.; Pala, M. G.; et al., *Semicond. Sci. Technol.* **26**, 6 (2011); Martins, F.; Hackens, B.; Pala, M. G.; et al., *Phys. Rev. Letters* **99**, 13 (2007)
- ¹⁰ M. G. Pala, B. Hackens, F. Martins, H. Sellier, V. Bayot, S. Huant and T. Ouisse, *Physical Review B* **77**, 125310 (2008)
- ¹¹ Fallahi P, Bleszynski A C, Westervelt R M, Huang J, Walls J D, Heller E J, Hanson M and Gossard A C, *Nano Lett.* **5** 223 (2005); Pioda A, Kiën S, Ihn T, Sigrist M, Fuhrer A, Ensslin K, Weichselbaum A, Ulloa S E, Reinwald M and Wegscheider W *Phys. Rev. Lett.* **93** 216801 (2004); Bleszynski-Jayich A C, Fröberg L E, Björk M T, Trodahl H J, Samuelson L and Westervelt R M *Phys. Rev. B* **77** 245327 (2008); L.M. Zhang and M.M. Fogler *Nano Lett.* **6**, 2206 (2006); Qian J, Halperin B I and Heller E J *Phys. Rev. B* **81** 125323 (2010) ; Boyd E E and Westervelt R M *Phys. Rev. B* **84** 205308 (2011).
- ¹² M. Ishikawa, M. Yoshimura and K. Ueda, *Journal of Applied Physics* **44**, 1502 (2005); S. Yoshimoto, Y. Murata, K. Kubo, K. Tomita, K. Motoyoshi, T. Kimura, H. Okino, R. Hobara, I. Matsuda, S. Honda, M. Katayama, and S. Hasegawa, *Nano Lett.* **7**, 956 (2007).
- ¹³ D. J. Kirkner and C. S. Lent, *Journal of Applied Physics* **67**, 6353 (1990)
- ¹⁴ M. Leng and C. S. Lent, *Journal of Applied Physics* **76**, 2240 (1994)
- ¹⁵ K. Kolasinski, B. Szafran, *Phys. Rev. B* **89**, 165306 (2014)
- ¹⁶ M. Zwierzycki, P. A. Khomyakov, A. A. Stariko K. Xia, M. Talanana, P. X. Xu, V. M. Karpan, I. Marushchenko, I. Turek, G. E. W. Bauer, G. Brocks, and P. J. Kelly, *Physica Status Solidi B* **245**, issue 4 p. 623-640 (2008)
- ¹⁷ V. A. Mandelshtam, T. R. Ravuri, and H. S. Taylor, *Phys. Rev. Lett.* **70**, 1932 (1993).
- ¹⁸ K. Kolasinski, B. Szafran, *New J. Phys.* **16**, 053044 (2014)
- ¹⁹ R. A. Jalabert, W. Szewc, S. Tomsovic, and D. Weinmann, *Phys. Rev. Lett.* **105**, 166802 (2010).
- ²⁰ C. Gorini, R. A. Jalabert, W. Szewc, S. Tomsovic, and D. Weinmann, *Phys. Rev. B* **88**, 035406 (2013).
- ²¹ N. Pascher, F. Timpu, C. Rössler, T. Ihn, K. Ensslin, C. Reichl, and W. Wegscheider, *Phys. Rev. B* **89**, 24508 (2014).
- ²² F. Martins, S. Faniel, B. Rosenow, M. G. Pala, H. Sellier, S. Huant, L. Desplanque, X. Wallart, V. Bayot, and B. Hackens, *New J. Phys.* **15**, 013049 (2013).
- ²³ K. Kolasinski, B. Szafran, and M. P. Nowak, *Phys. Rev. B* **90**, 165303 (2014).